Available online at www.sciencedirect.com
ScienceDirect
Engineering Structures 29 (2007) 1929–1938
ENGINEERING STRUCTURES
www.elsevier.com/locate/engstruct

Experimental and analytical investigation of tubular links for eccentrically braced frames

Jeffrey W. Berman[a,*], Michel Bruneau[b,c]

[a] Department of Civil and Environmental Engineering, More Hall 201-Box 352700, University of Washington, Seattle, WA 98195-2700, United States
[b] MCEER, University at Buffalo, Amherst, NY 14261, United States
[c] Department of Civil, Structural, and Environmental Engineering, University at Buffalo, Amherst, NY 14260, United States

Received 14 June 2006; received in revised form 11 October 2006; accepted 15 October 2006
Available online 30 November 2006

Abstract

Eccentrically braced frames have been used as seismic load resisting systems in buildings for more than two decades. Typically, the links, which are relied upon for energy dissipation through inelastic deformation, have had a wide-flange or I-shaped cross-section that requires lateral bracing to prevent lateral torsional buckling. This has limited the use of eccentrically braced frames in bridge piers and towers, as lateral bracing is difficult to provide in those situations. This paper describes first an experimental, and then an analytical investigation into the use of members with hollow rectangular (i.e., tubular) cross-sections as eccentrically braced frame links that do not require lateral bracing. Using cross-sectional plastic analysis, the plastic shear and moment strength for a general tubular section with different web and flange yield strengths and thicknesses are derived. Equations are derived for maximum flange compactness ratio and minimum web stiffener spacing to prevent flange and web buckling. A proof-of-concept experiment involving a large scale eccentrically braced frame with a tubular link is then described. The link has a hybrid tubular cross-section composed of webs and flanges of different thicknesses, with full-penetration groove welds. Experimental results indicate that the link reached a rotation of 0.15 rad, almost twice the current 0.08 rad limit for wide-flange links, prior to suffering flange fracture. An investigation of the fracture surface indicated that flange fracture did not initiate in the full-penetration weld used to assemble the shape, but rather in the heat-affected-zone of the flange adjacent to a fillet weld used to connect a stiffener to the flange. Finally, a finite element model of the link is developed using shell elements, and reasonable agreement with the experimental results is observed.

Keywords: Steel structures; Eccentrically braced frames; Experimental study; Earthquake engineering; Ductility

1. Introduction

Eccentrically braced frames (EBFs) have been used for more than two decades as a seismic load resisting system, primarily in buildings. This system, which relies on the yielding of a link beam between eccentric braces, has been shown to provide ductility and energy dissipation under seismic loading, and its behavior in various configurations has been investigated [1–10]. There are now well established guidelines for EBF design with wide-flange (WF) links in the AISC Seismic Provisions [11], referred to herein as *the Provisions*. However, the use of wide-flange shapes as link beams necessitates that they be braced out-of-plane to prevent lateral torsional buckling.

Recently, interest in the use of EBFs or energy dissipation systems with WF or I-shaped links has increased in bridge piers or towers; such systems have been designed, tested, and implemented for the San Francisco–Oakland Bay Bridge and the Richmond–San Rafael Bridge [12,13]. In these cases, special considerations for link stability were made that may have increased the cost of the projects. Therefore, it seems that the development of a link type that does not require lateral bracing is desirable for application of EBFs in bridge piers. Links of this type would also be useful in situations in buildings or other structures where lateral bracing may not be feasible or easily provided. Furthermore, the design of EBFs to protect

* Corresponding author. Tel.: +1 206 616 3530; fax: +1 206 543 1543.
E-mail addresses: jwberman@eng.buffalo.edu (J.W. Berman), bruneau@mceermail.buffalo.edu (M. Bruneau).

0141-0296/$ - see front matter © 2006 Elsevier Ltd. All rights reserved.
doi:10.1016/j.engstruct.2006.10.012

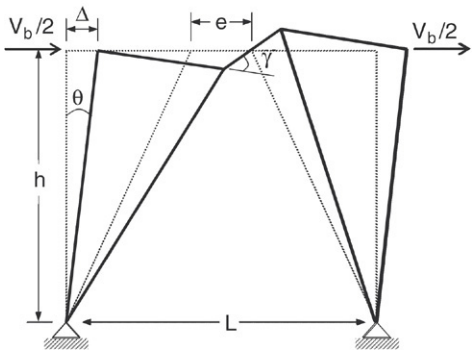

Fig. 1. Typical deformed eccentrically braced frame.

existing pier bracing members may be employed using the approach in Berman and Bruneau [14], or EBF systems may be used to replace existing deficient pier brace systems.

This paper describes the initial development of links with hollow rectangular (i.e., tubular) cross-sections for EBFs. Tube shapes have substantial torsional stability, making them less susceptible to lateral torsional buckling, and may thus not require lateral bracing. First, design equations are derived for plastic shear and moment capacity, as well as compactness and stiffener requirements. Then, a proof-of-concept experimental study on a single panel EBF utilizing a tubular link is described, followed by the modeling of that proof-of-concept link using finite elements. That calibrated model can serve as the basis for finite element parametric studies to examine the compactness requirements for tubular links [15,16].

2. Design equations

Prior to giving equations that are specific to tubular links, a brief review of the kinematics of a common EBF configuration is provided. Consider an EBF in an inverted chevron configuration, as shown in Fig. 1, where the link with length e deforms inelastically and resists the applied base shear, V_b, while the framing outside the link is designed to remain elastic. For this configuration, the base shear capacity of the frame can be written in terms of the plastic link shear strength, V_p, as:

$$V_b = V_p \frac{L}{h} \tag{1}$$

where L is the frame width and h is the frame height. The drift angle of the frame, θ, can then be written in terms of the link rotation angle, γ, as:

$$\theta = \gamma \frac{e}{L} \tag{2}$$

where deformations of the framing outside the link have been neglected, which is reasonable considering that the link may be subjected to large inelastic deformations while the surrounding framing remains essentially elastic.

Consider the generic tubular link cross-section shown in Fig. 2, where the webs and flanges may have different thicknesses and yield strengths. Using plastic cross-sectional

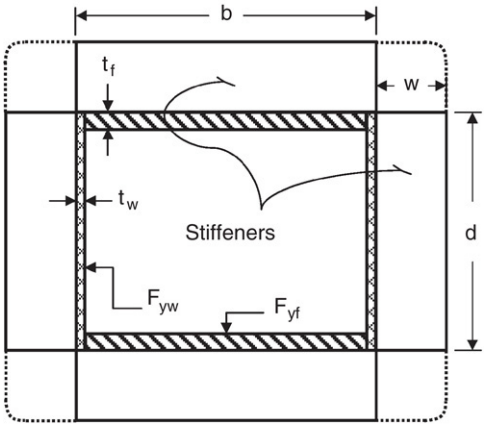

Fig. 2. Generic tubular cross-section with exterior stiffeners.

analysis, the plastic shear strength, V_p, of such a cross-section can be written as:

$$V_p = \frac{2}{\sqrt{3}} F_{yw} t_w (d - 2t_f) \tag{3}$$

where F_{yw} is the web yield strength, t_w is the web thickness, d is the web depth, and t_f is the flange thickness. The plastic moment strength of the cross-section can similarly be derived as:

$$M_p = F_{yf} t_f (b - 2t_w)(d - t_f) + F_{yw} \frac{t_w d^2}{2} \tag{4}$$

where F_{yf} is the flange yield strength, b is the flange width, and the other parameters are as previously defined. Note that the web-flange intersection regions at the corners of the cross-section have not been included in the plastic shear strength of Eq. (3). This assumption is consistent with the plastic shear strength formulation for WF shapes in *the Provisions* [11]. Similarly, the plastic moment capacity considering only the effect of the flanges, implying that the webs have fully yielded in shear and cannot contribute to the moment capacity, known herein as the reduced plastic moment, M_{pr}, is:

$$M_{pr} = F_{yf} t_f (b - 2t_w)(d - t_f) + 2F_{yw} t_f t_w (d - t_f) \tag{5}$$

where all terms are as previously defined.

WF links are categorized in terms of their predominant yielding mechanism (i.e., shear or flexural yielding) based on the relationship between shear and moment capacity, and link length. Defining the normalized link length, ρ, as:

$$\rho = \frac{e}{(M_p / V_p)} \tag{6}$$

the classification of WF links by the AISC Seismic Provisions is as follows:

- Links with $\rho \leq 1.6$ are shear links that yield predominantly in shear and have a maximum link rotation under the design seismic loading of 0.08 rad;
- Links with $\rho > 2.6$ are flexural links that yield predominantly in flexure and have a maximum link rotation under the design seismic loading of 0.02 rad; and

- Links with $1.6 < \rho \leq 2.6$ are intermediate links that may have significant shear and flexural yielding, and have a maximum link rotation under the design seismic loading that can be found through linear interpolation using the above link lengths and maximum rotations (note that $\rho = 2.0$ indicates simultaneous achievement of both V_p and M_p and the corresponding link length is denoted as the balanced link length).

For the research described in this paper regarding links having tubular cross-sections, the above normalized link length, behavior classification, and corresponding rotation limits are also adopted (i.e., the methods used to determine them for WF links are applicable to tubular cross-sections as well [15]).

Taking into consideration the above rotation limits and the relationship between link rotation and frame drift given by Eq. (2), built-up or hybrid tubular shapes (hybrid meaning those with webs and flanges having different yield strengths) might be necessary in bridge applications. Indeed, using the hollow structural sections listed in the AISC Manual of Steel Construction [17] that also meet the limits for compactness ratio in *the Provisions*, the maximum link length for a shear link as defined above is 460 mm, and is obtained with a HSS $250 \times 250 \times 16$. Considering a single panel, or storey, of a representative bridge pier that is 7.3 m wide and 3.7 m tall with such a short link, the drift at a link rotation of 0.08 rad would be only 0.5% (from Eq. (2)). It is conceivable that drift demands would exceed this relatively small value. Furthermore, the EBF stiffness and fundamental period of vibration are largely controlled by the link length, and EBFs with excessively short links may have large stiffnesses, corresponding to larger base shear forces. To avoid these problems, a built-up and/or hybrid cross-section can be employed, so that longer link lengths can be used while still maintaining shear link behavior and the associated larger maximum rotations.

Local buckling of webs and/or flanges has been shown to be detrimental to the ductility of WF links. It can be assumed that same would be true of tubular links. As such, it is necessary to develop compactness requirements that enable tubular links to achieve the desired ductility (i.e., rotation levels) prior to significant strength degradation. For this purpose, a maximum flange compactness ratio and maximum stiffener spacing equation for web stiffeners were derived in Berman and Bruneau [15], and these are summarized below.

2.1. Flange compactness ratio

Flange buckling of links in EBFs can lead to high strains, which in turn can cause premature fractures as well as trigger lateral torsional buckling or web buckling, all of which cause significant strength degradation and limit ductile behavior. Kasai and Popov [7] derived a limiting flange compactness ratio (b/t_f) for which flange buckling could be avoided in WF links, and compared that to the limit given for plastic design in the then current AISC Allowable Stress Design Specifications [18]. They found that the codified limit was slightly conservative, but recommended that it also be used as the limit for WF EBF links. Since then, test results under larger cyclic rotations have resulted in the reduction of the limit flange compactness ratio for WF links [11].

A similar approach to that used for WF links by Kasai and Popov can be followed to assess the flange buckling of a hollow rectangular section of the type shown in Fig. 2. First the flange yield length is determined. This value is then introduced in a plastic plate buckling equation to determine the critical buckling stress of the flange element, which in turn is compared with an estimate of the average flange stress in the flange yield zone. Limiting the average flange stress to the critical buckling stress and solving for b/t_f gives:

$$\frac{b}{t_f} \leq 1.02\sqrt{\frac{E}{F_{yf}}}. \tag{7}$$

Note that this derivation does not account for cyclic stresses and strains. Additional details of this derivation can be found in Berman and Bruneau [15].

The current compactness ratio limits for tube shapes in *the Provisions* are from work by Lee and Goel [19] and Hassan and Goel [20] on fracture and local buckling prevention in concentrically braced frames. They are based on test results using hollow rectangular and square members in compression, or in combined compression and flexure. Comparing that current limit in *the Provisions*:

$$\frac{b}{t_f} \leq 0.64\sqrt{\frac{E}{F_{yf}}} \tag{8}$$

with the limit in Eq. (7) suggests that the current limit is theoretically conservative for use in the design of EBF links with tubular cross-sections, when cyclic strain accumulation is neglected.

2.2. Stiffener spacing

Web buckling of links in EBFs cause rapid strength and stiffness degradation, and this significantly impedes the energy dissipation capabilities of the system. Web stiffeners can be used to delay web buckling beyond a certain rotation level. Kasai and Popov [7] derived the stiffener spacing formula for WF links that appears in *the Provisions*.

Fully restrained boundary conditions for the web sides adjacent to the flanges were used in the Kasai and Popov derivation because of the presence of flange sections on both sides of the web and the high moment gradient. In the case of a hollow rectangular cross-section, there is flange on only one side of each web in the lateral direction, and, simply supported boundary conditions are assumed (as traditionally considered for web buckling considerations in plate and box girders [21]).

The limiting panel aspect ratio, α, for tubular links (i.e., the stiffener spacing, a, divided by the web depth, d) can be found using a similar procedure to that used by Kasai and Popov for WF links as [15]:

$$\alpha = \sqrt{\frac{5.34}{\left(\frac{\gamma_u \beta^2}{4.35}\right) - 4}} \tag{9}$$

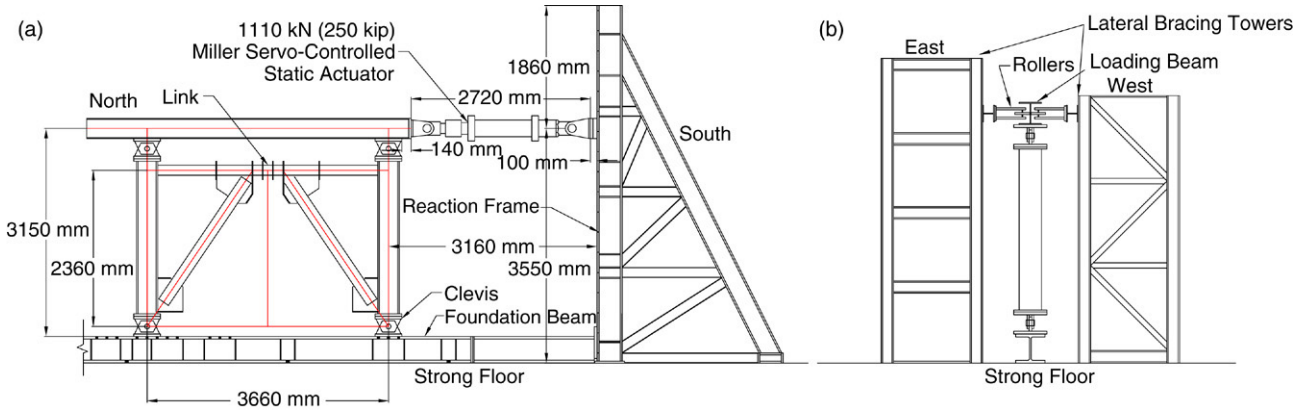

Fig. 3. Proof-of-concept test setup (a) elevation (b) plan.

where γ_u is the maximum rotation of the link and β is the web compactness ratio, i.e., the clear web depth, $d - 2t_f$ divided by the web thickness, t_w. This equation can be conservatively approximated by:

$$\frac{a}{t_w} + \frac{1}{8}\frac{d}{t_w} = C_B \quad (a \le d) \tag{10}$$

where C_B is 20 and 37 for ultimate link rotations of 0.08 rad (which is the maximum allowed for WF links in *the Provisions*) and 0.02 rad respectively, and the web depth $(d - 2t_f)$ has been conservatively replaced by the section depth d. The above stiffener spacing requirements are applicable for shear and intermediate links ($\rho \le 2.6$) with tubular cross-sections. For flexural links ($\rho > 2.6$) with tubular cross-sections, stiffeners are not necessary [16].

2.3. Stiffener sizing

Stiffeners for tubular links may be positioned around the outer perimeter of the cross-section as shown in Fig. 2. Configurations with stiffeners inside the tube are also possible if attached only to the webs, which is acceptable, as stiffeners have been found to have no significant impact on flange buckling [16]. The latter configuration may be more desirable for bridge applications, as it would reduce the number of locations that could serve as collectors for moisture and debris. The design requirements for internal stiffeners would be similar to those given below for external stiffeners. The specific selection of the stiffener configuration will depend on aesthetic requirements, usage (i.e., bridges or buildings), inspection requirements, as well as the intended duration of the service life of the structure. Vertical web stiffeners for tubular links are eccentrically loaded, in that the load they must resist is applied at half the stiffener width, w, from the stiffener's center. Salmon and Johnson [21] showed that eccentrically loaded stiffeners for plate girders should be designed for the stiffener compression force, P_s, from:

$$P_s = \frac{1}{2}\sigma_t t_w a \left(1 - \frac{\frac{a}{d}}{\sqrt{1 + \left(\frac{a}{d}\right)^2}}\right) \tag{11}$$

where σ_t is a tension field stress taken as the ultimate strength of the web, F_{uw}, and the other terms are as previously defined. Setting this stiffener force equal to the stiffener yield force, $A_{st}F_{ys}$, where F_{ys} is the stiffener yield strength and A_{st} is the stiffener area, the minimum stiffener area can be found to be:

$$A_{st} = \frac{F_{uw}t_w a}{0.828F_{yst}}\left(1 - \frac{\frac{a}{h}}{\sqrt{1 + \left(\frac{a}{h}\right)^2}}\right). \tag{12}$$

Additionally, to prevent stiffener buckling, web stiffeners should satisfy the minimum moment of inertia requirements given in Appendix F2.3 of the AISC LRFD Specifications [17], namely:

$$I_{st} \ge jat_w^3 \quad \text{where } j = \frac{2.5}{(\frac{a}{d})^2} \ge 0.5 \tag{13}$$

and I_{st} is the stiffener inertia taken about the web, i.e. $t_s w^3/3$, and t_s is the stiffener thickness.

3. Proof-of-concept testing

3.1. Setup and specimen design

To investigate the use of tubular cross-sections for links in EBFs where no lateral bracing of the link is provided, a proof-of-concept single storey (or single panel in the context of a bridge pier) EBF was designed and quasi-statically tested in the Structural Engineering and Earthquake Simulation Laboratory (SEESL) at the University at Buffalo. Due to the constraints of available equipment in the SEESL, the overall test specimen dimensions were set to a height of 3150 mm and width, L, of 3660 mm. The test setup is shown in Fig. 3. As shown, a hydraulic actuator applied horizontal force to a loading beam that equally distributed the load to clevises at the top of each column (a small variation in the load to each column is expected due to the axial flexibility of the loading beam). The frame was mounted on clevises at the base of each column that were fastened to a foundation beam that attached to the strong floor of the SEESL and also to the reaction frame where the actuator was mounted. For safety, the setup was globally braced for out-of-plane stability at two points on the loading

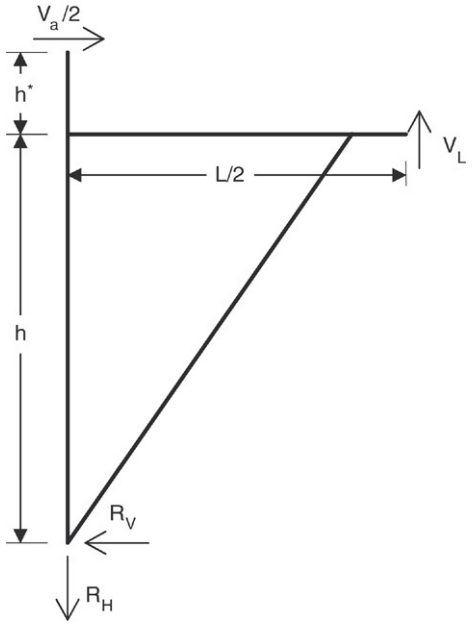

Fig. 4. Test setup free-body diagram.

beam by using the towers available in the SEESL, as shown in Fig. 3(b); however, no lateral bracing was provided to the link itself. Specifically, there were no elements included to resist compression flange instability in the link beam, except those that would be there in actual bridge piers, namely the eccentric braces and columns. Further, the global out-of-plane stability provided by the lateral bracing towers to the frame is similar to what would be provided to piers by the longitudinal stiffness of a bridge superstructure.

Excluding the loading beam and clevis heights, the actual height of the specimen from the centerline of the link beam to the centerline of the lower clevises, h, was set at 2360 mm. Denoting the distance from the centerline of the link beam to the centerline of the upper clevises as h^*, assuming zero moments at the clevis centerlines and the middle of the link, and assuming that the actuator load is evenly distributed to the two columns, the free body diagram of Fig. 4 can be used to determine the link shear force, V_L, in terms of the applied actuator load, V_a, as:

$$V_L = V_a \frac{h + h^*}{L}. \tag{14}$$

The hybrid link must be designed to satisfy several conditions simultaneously. It must have the desired shear strength, flexural strength, and link length, while meeting the limits for flange compactness (b/t_f) and web compactness (d/t_w) for HSS sections from *the Provisions*. Additionally, a frame drift-to-link rotation ratio must be selected so that adequate energy dissipation can be achieved prior to the link rotation reaching 0.08 rad. In this proof-of-concept test, it was decided to test a shear link, as these were deemed more likely to be used in practical applications (partly due to their larger rotation limits). Finally, the beam outside the link must be able to resist large axial forces and moments acting simultaneously.

More specifically, the link cross-section for the experimental test specimen was sized as follows:

- To ensure that the actuator would have the capacity to push the specimen well into the strain hardening range, and to account for material yield stresses that may be larger-than-specified, the maximum applied force, V_a, was set to 445 kN.
- Using Eq. (14), the required link shear force, V_L, was found to be 327 kN for V_a of 445 kN, h of 2360 mm, and h^* of 326 mm.
- The required shear area, $A_s = (d - 2t_f)t_w$, was found to be 880 mm^2 from Eq. (3), rearranged as:

$$(d - 2t_f)t_w = \frac{\sqrt{3}V_p}{2\phi_v F_y}. \tag{15}$$

  Note that a resistance factor, ϕ_v, of 0.9 was considered, the link plastic shear force V_p was taken as V_L from above, and the yield stress, F_y, was assumed to be 345 MPa.
- Next, the minimum link length was determined to achieve a link rotation, γ_u, of 0.08 rad at a minimum drift, Δ/h, of 1%. Using the following relationship for link length, drift, link rotation, and bay width [22]:

$$\frac{\Delta}{h} = \gamma_u \frac{e}{L} \tag{16}$$

  the minimum link length was determined to be 460 mm (18 in.).
- Next, the maximum shear link length, e^*, was determined from Eq. (6). Here, ρ was taken as 1.6 and the plastic moment was multiplied by a resistance factor, ϕ_b, of 0.9. Additionally, the plastic shear was multiplied by the R_y for A572 Grade 50 steel of 1.1, which is the ratio of expected to specified yield stress [11]. The resulting conservative equation for the maximum shear link length was:

$$e^* = \frac{1.31 M_p}{V_p}. \tag{17}$$

- Assuming a yield stress of 345 MPa, and using the results of Eq. (16) to define the minimum link length, the results of Eq. (17) to define the maximum link length (to maintain a shear link), the results of Eq. (15) for the minimum required shear area, and the limits of *the Provisions* for both web and flange compactness, given by:

$$\frac{b - 2t_w}{t_f} \quad \text{or} \quad \frac{d - 2t_f}{t_w} \le 0.64\sqrt{\frac{E}{F_y}} \tag{18}$$

  the following link cross-section dimensions and length were chosen: $d = b = 150$ mm, $t_f = 16$ mm, $t_w = 8$ mm, and $e = 460$ mm. Using these values, the anticipated plastic shear force, plastic moment, and plastic base shear were 381 kN, 120 kN m, and 519 kN, respectively.

To put the design strength of this proof-of-concept link in perspective, it is useful to consider the demands required for bridge piers considered in other research. The plastic shear force of 381 kN is approximately twice the link shear that would be required for implementation of an EBF in the two storey (i.e., two panels tall) single bay pier considered in Pollino and

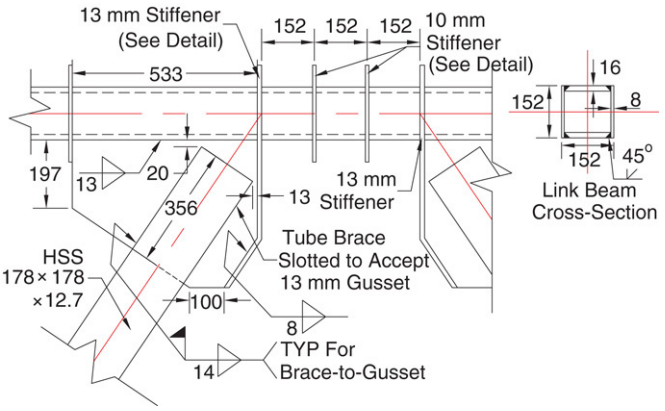

Fig. 5. Proof-of-concept link details.

Bruneau [23]. That pier was for a two-lane slab on girder bridge with simple spans, and was based on a survey of various bridges with steel piers around the United States and Canada; it is a relatively small pier. The required link shear was determined using the equivalent lateral force procedure and assuming an response modification value, R, of 6 [24]. Furthermore, the design link plastic shear force for the proof-of-concept test is 1/4 and 1/6 of the design link shear force for the San Francisco–Oakland Bay Bridge piers [12] and Richmond–San Rafael Bridge piers [13], respectively. Therefore, taking into consideration that these two are large bridges in high seismicity areas, the link designed for the proof-of-concept test seems to be of reasonable scale.

The steel specified for the link was A572 Gr. 50, which has a nominal yield strength of 345 MPa. Framing outside the link was designed to remain elastic using the procedure in Naiem [25], and it was designed considering a link shear force of twice the nominal plastic shear of 381 kN to account for strain hardening and the possibility of larger-than-specified steel yield strengths. Braces were HSS 178 × 178 × 12.7 (US-7 × 7 × 1/2) and columns were W 310 × 143 (US-12 × 96) and the beam-to-column, brace-to-column, and brace-to-beam connections were all designed to be moment resisting.

Link details are shown in Fig. 5. The link stiffener spacing and stiffener sizes were designed using the equations presented above. From Eq. (10), a stiffener spacing of 150 mm was calculated, then using Eqs. (12) and (13), a minimum stiffener thickness of 10 mm and minimum stiffener width of 64 mm were selected. Note that the stiffener width (i.e., the distance from the surface of the link to the edge of the stiffener), was kept constant around the entire cross-section. Assuming ASTM A572 Gr. 50 steel with a yield stress of 345 MPa is used for the stiffeners, a 6.5 mm fillet weld on both sides of each stiffener and all-around the link-to-stiffener interface, was designed to resist the full yield strength of the stiffeners.

It may be possible to design fillet welds for the connection of the web plates to the flange plates. For such a design, the equilibrium of a section of flange near the end (where it is fully plastified), should be considered, as shown in Fig. 6. Assuming that the change in moment over the length of link is linear, a reasonable assumption considering the effects of strain hardening, the shear flow that must be transmitted to the webs

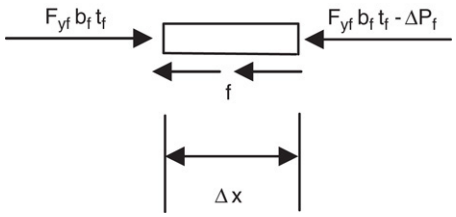

Fig. 6. Flange free-body diagram for shear flow.

through the welds, f, can be found from:

$$f = \frac{\Delta P_f}{\Delta x} = \frac{2F_{yf} b_f t_f}{e} = \frac{2V_p F_{yf} b_f t_f}{\rho M_p} \tag{19}$$

where ΔP_f is the change in flange force over the length Δx. Additionally, the ratio of mean to nominal flange yield stress should be considered (i.e., R_y from [11]), as should the likely flange overstrength from strain hardening, which can conservatively be taken as 1.3 for $\rho \leq 1.6$ and 1.5 otherwise [16].

For the proof-of-concept test specimen, a full penetration groove weld was chosen to join the 4 plates (2 webs and 2 flanges) that were used to build the link's hybrid cross-section. This ensures the development of the full strength of the material and does not require a shear flow calculation. As shown in Fig. 5, the flanges were designed with 45° bevels to accommodate the full penetration groove weld. This detail was selected over one in which the webs were beveled because, the flanges being thicker than the web, it allowed for a larger base-metal to weld-metal contact area for the same bevel angle. However, alternate details to the one in Fig. 5 are possible.

All plates for the link beam were specified to be ASTM A572 Grade 50 steel, and compliance was verified by a review of the mill certificates. The two web plates were cut from the same original 16 mm thick plate; similarly, the two flange plates were cut from a single 8 mm thick plate. Coupons for tension testing conforming to ASTM standards [26] were fabricated from both the flange and web plate materials. Mean coupon test results are shown in Fig. 7 for both the web and flange materials. Note that the yield stress for the web material, 448 MPa, is considerably higher than the 345 MPa specified, while the yield stress of the flange material, 393 MPa, is closer to the specified value (and slightly exceeding the expected yield strength of 380 MPa for this steel grade) [11]. Using the results of the coupon tests, the link plastic shear, V_p, and plastic moment, M_p, were determined to be 495 kN, and 157.6 kN m, respectively.

3.2. Experimental loading

The quasi-static loading protocol used here was developed based on the guidelines presented in ATC-24 [27]. The cycles up to and including yielding were performed under force control. Verification of the yield force was carried out by checking the values for the principal strains from the rosettes on the web of the link; the displacement of the specimen at the first occurrence of that force was assigned to be the yield displacement. Beyond yield, the subsequent cycles

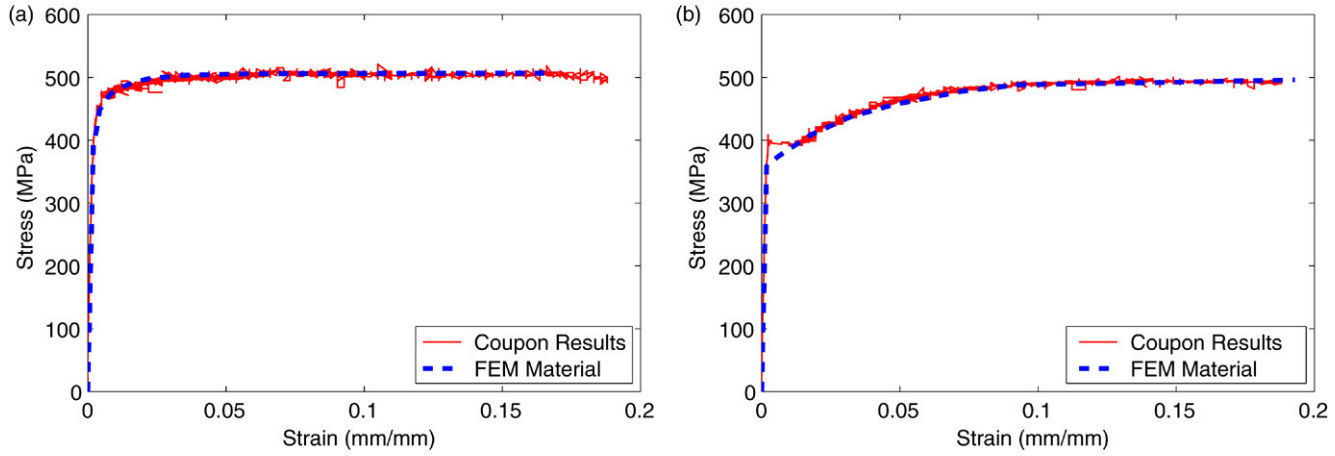

Fig. 7. Stress–strain curves (a) web material (b) flange material.

Table 1
Loading history for proof-of-concept test

Cycle no.	Fraction of δ_y	Drift (%)	γ (rad)	V_a (kN)	V_L (kN)
1	0.33	0.11	0.004	213	157
2	0.33	0.11	0.004	217	159
3	0.33	0.11	0.004	212	156
4	0.67	0.23	0.008	434	319
5	0.67	0.23	0.008	432	318
6	0.67	0.24	0.009	445	327
7	1.0	0.38	0.014	668	491
8	1.0	0.37	0.013	646	475
9	1.0	0.37	0.013	664	488
10	2.0	0.76	0.038	842	619
11	2.0	0.75	0.037	850	625
12	2.0	0.75	0.037	853	627
13	3.0	1.15	0.067	893	656
14	3.0	1.14	0.066	912	671
15	3.0	1.14	0.066	912	670
16	4.0	1.54	0.096	947	696
17	4.0	1.52	0.093	956	703
18	5.0	1.92	0.123	991	728
19	5.0	1.92	0.123	996	733
20	6.0	2.30	0.151	1009	742

were applied in displacement control using the horizontal displacement recorded at the link beam level. Table 1 gives the recorded values of maximum base shear (obtained from the actuator load cell output), V_a, the calculated values of percent drift and link rotation, γ, and the corresponding fraction of the yield displacement for each cycle imposed on the specimen.

It should be noted that in some previous tests by others on EBF links alone, or on link-brace-column assemblies [12,13,28], the loading protocol from the 2002 AISC Seismic Provisions [29] for the testing of link-to-column connections has been used (this loading protocol has been revised in the 2005 Edition of the Provisions based on the work in [30]). It should be noted that the 2002 AISC protocol would have resulted in more cycles of rotations in the inelastic range. In conducting additional testing on tubular links alone, the authors used both the original and revised AISC protocols [16]. However, since an entire EBF was tested here, and because the behavior of the framing outside the link was also of interest, it

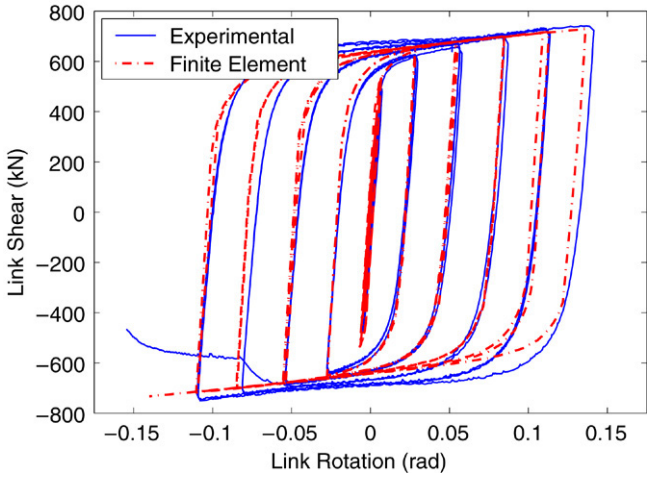

Fig. 8. Comparison of experimental and analytical link shear versus link rotation hysteresis curves.

was decided that the ATC recommendations were appropriate, since they are based on frame drift.

3.3. Experimental results

The initial stiffness of the specimen was determined to be 80 kN/mm from the elastic cycles. The yield drift was identified as 0.37% and corresponded to a base shear of 668 kN, while the maximum base shear and drift reached were 1009 kN and 2.3%, respectively. Fig. 8 shows the corresponding link shear force vs. link rotation hysteresis. The link shear at yield, V_{ye}, and corresponding yield rotation were 490 kN and 0.014 rad respectively, while the maximum link shear, $V_{\max e}$, and rotation were 742 kN and 0.151 rad, respectively (note that the maximum rotation for which a complete cycle was achieved was 0.123 rad). Taking into consideration projections of the elastic and inelastic slopes of Fig. 8, the plastic shear force, V_{pe}, was approximately 520 kN and the link shear force at a link rotation of 0.08 rad, $V_{0.08e}$, the current limit for EBFs in buildings, was 689 kN. The ratios of the experimentally obtained values of link shears at those various points in the loading history to the design link plastic shears and the link

Table 2
Ratios of experimentally obtained link shear forces and moments to capacities calculated using design and actual material properties

	V_p		
	V_{pd} (381 kN)	V_{pa} (495 kN)	V_{pu} (564.2 kN)
V_{ye}/V_p	1.29	0.99	0.86
V_{pe}/V_p	1.36	1.05	0.92
$V_{0.08e}/V_p$	1.81	1.39	1.22
$V_{\max e}/V_p$	1.95	1.50	1.32
	M_p		
	M_{pd} (120 kN m)	M_{pa} (158 kN m)	M_{pu} (192 kN m)
M_{ye}/M_p	0.93	0.71	0.58
M_{Vpe}/M_p	0.99	0.76	0.62
$M_{0.08e}/M_p$	1.32	1.00	0..82
$M_{\max e}/M_p$	1.42	1.08	0.89
	M_{pr}		
	M_{prd} (114 kN m)	M_{pra} (132 kN m)	M_{pru} (162 kN m)
M_{ye}/M_{pr}	0.98	0.85	0.69
M_{Vpe}/M_{pr}	1.04	0.90	0.73
$M_{0.08e}/M_{pr}$	1.39	1.20	0.97
$M_{\max e}/M_{pr}$	1.49	1.29	1.05

plastic shears calculated using actual material properties (both yield and ultimate stresses) are given in Table 2. In that table, V_{pd} is the plastic shear calculated using the design yield stress, V_{pa}, is the plastic shear calculated using the actual yield stress, and V_{pu}, is the plastic shear calculated using the ultimate material stresses. Recall from Fig. 7 that the yield and ultimate stresses of the web material, F_{yw} and F_{uw}, were found to be 448 MPa and 510 MPa respectively, and that the yield and ultimate stresses of the flange material, F_{yf} and F_{uf}, were found to be 393 MPa and 490 MPa, respectively.

The experimentally obtained values of link end moments, calculated from the link shear using $M_L = V_L e/2$, at specimen yield, M_{ye}, development of V_p, M_{Vpe}, and 0.08 rad of link rotation, $M_{0.08e}$, were 112 kN m, 119 kN m, and 158 kN m, respectively, while the maximum end moment reached during the test, M_{ue}, was 170 kN m. Table 2 presents the ratios of those experimentally obtained values of link end moment to the link plastic moment calculated using the design yield stresses, M_{pd}, actual yield stresses, M_{pa}, and ultimate material stresses, M_{pu}. Additionally, the table presents those same ratios found using the reduced plastic moments, M_{prd}, M_{pra}, and M_{pru}, from Eq. (5) with the design yield stress, actual yield stress, and actual ultimate stress, respectively.

As shown in Table 2, the maximum link shear obtained was 1.5 times the plastic shear strength determined using the actual web yield stress. This is similar to the overstrength observed for WF shear links, and is likely due to the presence of shear in the flanges as well as the webs [31,16]. Additionally, the plastic moment capacity calculated using the actual material yield stresses was also exceeded. This indicates that, due to strain hardening, the shear–moment interaction can be neglected and both V_p and M_p can be achieved. A similar conclusion was reached for WF links by Kasai and Popov [7].

The link deformed at the peak of the negative excursion of Cycle 19 (0.123 rad link rotation) is shown in Fig. 9(a). No buckling of the webs or flanges was observed, indicating that the compactness ratios and stiffener spacing used for this proof-of-concept link (which met the AISC prescribed limits, which are incidentally lower than those derived in Section 2), were adequate to prevent local buckling prior to achieving large rotations. Additionally, there was no evidence of lateral torsional buckling, and the out-of-plane moments for the beam-outside-the-link and in the eccentric braces, as determined from strain gauge measurements, never exceeded 2.5% of the nominal link plastic moment, and could easily have been caused by accidental eccentricities resulting from fabrication.

The failure mode of the link was the fracture of the bottom flange after completing a half-cycle at 0.151 rad (almost twice the maximum link rotation allowed by the AISC Seismic Provisions). This fracture is shown in Fig. 10(a) and the fracture surface examined after testing is shown in Fig. 10(b). Factors that likely contributed to this are the large plastic strain demands at that location, the high degree

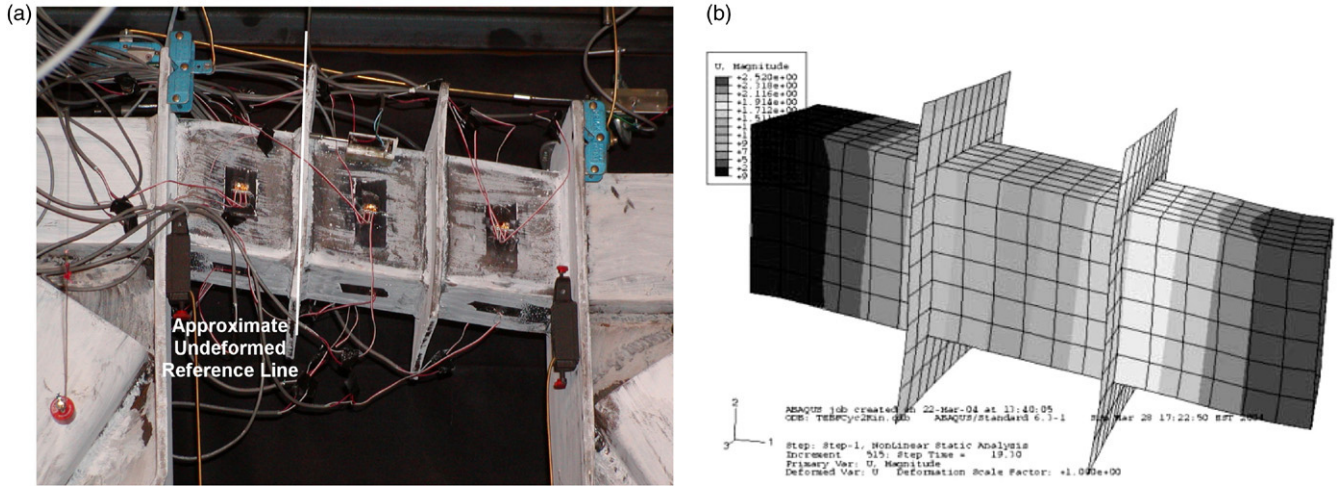

Fig. 9. Deformed link at 0.123 rad during Cycle 19 (a) experimental (b) finite element analysis results.

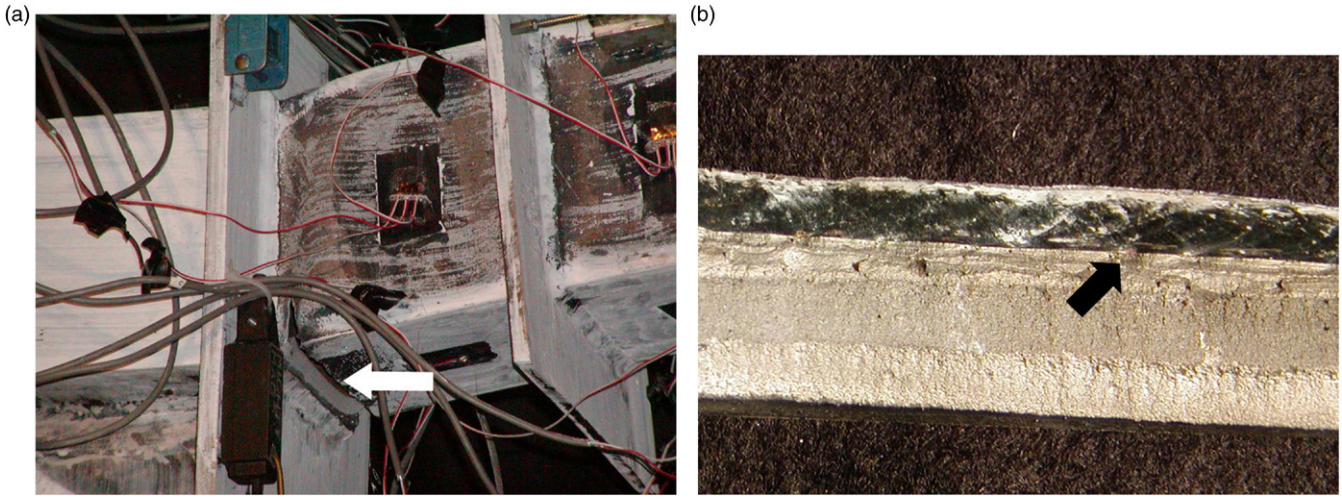

Fig. 10. (a) Link fracture at 0.151 rad during Cycle 20 (b) fracture surface exposed after testing.

of constraint due to the presence of the gussets, stiffeners, and welds used for the link-to-brace connection, and heat-affected-zone (HAZ) brittleness near the gusset-stiffener weld. Inspection of the failure surface was performed using a magnifying glass and light-microscope with 30x magnification (personal communication, Mark Lukowski, metallurgist, and Dr. Robert C. Wetherhold, mechanical engineer, Department of Mechanical and Aerospace Engineering, University at Buffalo, September 2003). The fracture was assessed as having been initiated by cracking in the previously described HAZ and the propagation of those cracks under load reversals. A likely starting point in a pitted area of the gusset-stiffener weld to the link flange is identified in Fig. 10(b). There was no evidence of crack initiation in the full penetration groove weld used to assemble the webs and flanges of the link.

4. Finite element modeling

A finite element model of the link from the proof-of-concept test was developed in ABAQUS [32]. Some preliminary analyses were conducted to study the effect of mesh refinement, and to determine whether reduced integration elements could be used to improve computational time without loss of significant accuracy.

The finite element model used shell elements to represent the webs, flanges, and stiffeners of the proof-of-concept link. An element edge length of approximately 25 mm was found to adequately represent the behavior of the link through a mesh refinement study. The resulting element edge to thickness ratios varied from 1.6 to 3.0. Reduced integration shell elements, denoted S4R in ABAQUS, were selected to improve computation time, and were found to have no noticeable impact on the results. Computation time is relevant to the use of this model for a finite element parametric study of different link geometries [16].

Boundary conditions similar to those employed by Richards and Uang [31] in their study of wide-flange links were used here. These boundary conditions allow axial deformation of the link while preventing rotation at both ends, thus being similar to the boundary conditions for the proof-of-concept link specimen. Loading is applied through the application of vertical displacement at the link end. In terms of horizontal and vertical nodal displacements, u_x and u_y respectively, and rotations, r_z, the boundary conditions used can be expressed as:

$$u_y(0) = r_z(0) = u_x(L) = r_z(L) = 0. \tag{20}$$

The nonlinear kinematic hardening plasticity material model available in ABAQUS was used in the finite element model of the proof-of-concept link. Only monotonic coupon test data were available for the materials used to fabricate the link; therefore these were input as half cycle data for the material model. The experimental stress–strain curves and ABAQUS stress strain curves are shown in Fig. 7(a) and (b) for the web and flange material, respectively. The flange material definition was also used for the stiffeners. No fracture model was employed in the finite element model of the proof-of-concept link.

As shown in Figs. 8 and 9, good agreement was obtained between the analytical and experimental results in terms of both their hysteretic behavior and overall deformation patterns. The stresses and strains at key locations in the finite element model were also near their expected values. Additionally, the model adequately captures the link overstrength, and can be used to check overstrength predictions from methods such as that in Richards and Uang [31].

5. Conclusions

A new link for eccentrically based frames that is self-stabilizing and does not require lateral bracing has been developed, tested, and modeled analytically. This link utilizes a hybrid tubular cross-section for which the strength equations, preliminary stiffener spacing, and compactness requirements have been derived. A proof-of-concept experiment showed that hybrid tubular links can achieve and exceed the maximum rotation for links specified in the AISC Seismic Provisions, indicating that they can provide ductility levels similar to those of wide-flange links. Design equations and requirements

have been proposed and, in a preliminary sense, verified by the successful testing of the proof-of-concept specimen. It was found that, at least for this specimen, its shear–moment interaction can be neglected, as both the plastic shear and plastic moment capacity of the cross-section, calculated using actual material properties, were exceeded due to strain hardening. Furthermore, the maximum link shear exceeded the plastic shear strength calculated using the ultimate stress of the web material, indicating that some shear was likely being carried by the flange as well. Finally, a finite element model of the proof-of-concept link was developed using shell elements and showed reasonable agreement in terms of deformations and hysteretic behavior.

Acknowledgments

This research was conducted by the State University of New York at Buffalo and was supported by the Federal Highway Administration under contract number DTFH61-98-C-00094 to the Multidisciplinary Center for Earthquake Engineering Research. However, any opinions, findings, conclusions, and recommendations presented in this paper are those of the authors and do not necessarily reflect the views of the sponsors.

References

[1] Roeder CW, Popov EP. Eccentrically braced steel frames for earthquakes. Journal of the Structural Division 1978;104(3):391–412.
[2] Roeder CW, Popov EP. Cyclic shear yielding of wide-flange beams. Journal of the Engineering Mechanics Division 1978;104(4):763–80.
[3] Popov EP, Bertero VV. Seismic analysis of some steel building frames. Journal of the Engineering Mechanics Division 1980;106(1):75–92.
[4] Hjelmstad KD, Popov EP. Cyclic behavior and design of link beams. Journal of Structural Engineering 1983;109(10):2387–403.
[5] Hjelmstad KD, Popov EP. Characteristics of eccentrically braced frames. Journal of Structural Engineering 1984;110(2):340–53.
[6] Malley JO, Popov EP. Shear links in eccentrically braced frames. Journal of Structural Engineering 1984;110(9):2275–95.
[7] Kasai K, Popov EP. Study of seismically resistant eccentrically braced steel frame systems. Report no. UCB/EERC-86/01. Earthquake Engineering Research Center; 1986.
[8] Kasai K, Popov EP. General behavior of WF steel shear link beams. Journal of Structural Engineering 1986;112(2):362–82.
[9] Ricles JM, Popov EP. Composite action in eccentrically braced frames. Journal of Structural Engineering 1989;115(8):2046–66.
[10] Engelhardt MD, Popov EP. Experimental performance of long links in eccentrically braced frames. Journal of Structural Engineering 1992; 118(11):3067–88.
[11] AISC. Seismic provisions for structural steel buildings. American Institute of Steel Construction; 2005.
[12] Dusicka P, Itani AM, Buckle IG. Cyclic behavior of shear links and tower shaft assembly of San Francisco–Oakland Bay bridge tower. Technical report CCEER 02-06. Center for Civil Engineering Earthquake Research; 2002.
[13] Itani AM. Cyclic behavior of Richmond–San Rafael tower links. Technical report CCEER 97-4. Center for Civil Engineering Earthquake Research; 1997.
[14] Berman JW, Bruneau M. Supplemental system retrofit considerations for braced steel bridge piers. Journal of Earthquake Engineering and Structural Dynamics 2005;34(4–5):497–517.
[15] Berman JW, Bruneau M. Approaches for the seismic retrofit of braced steel bridge piers and proof-of-concept testing of a laterally stable eccentrically braced frame. Technical report MCEER-05-0004. Multidisciplinary Center for Earthquake Engineering Research; 2005.
[16] Berman JW, Bruneau M. Further development of tubular eccentrically braced frame links for the seismic retrofit of braced steel truss bridge piers. Technical report MCEER-06-0006. Multidisciplinary Center for Earthquake Engineering Research; 2006.
[17] AISC. Manual of steel construction: Load and resistance factor design. 3rd ed. American Institute of Steel Construction; 2001.
[18] AISC. Manual of steel construction. 8th ed. Chicago: American Institute of Steel Construction; 1980.
[19] Lee S, Goel SC. Seismic behavior of hollow and concrete-filled square tubular members. Technical report UMCE 87-11. University of Michigan Department of Civil Engineering; 1987.
[20] Hassan OF, Goel SC. Modeling of bracing members and seismic behavior of concentrically braced steel structures. Technical report UMCE 91-1, University of Michigan Department of Civil Engineering; 1991.
[21] Salmon CG, Johnson JE. Steel structures — design and behavior. 4th ed. New York: HarperCollins College Publishers; 1996.
[22] Bruneau M, Uang CM, Whittaker AS. Ductile design of steel structures. New York: McGraw-Hill; 1998.
[23] Pollino MC, Bruneau M. Seismic retrofit of bridge steel truss piers using a controlled rocking approach. Technical report MCEER-04-0011. Multidisciplinary Center for Earthquake Engineering Research; 2004.
[24] FEMA. NEHRP recommended provisions for seismic regulations for new buildings and other structures, FEMA 450. Building Seismic Safety Council for the Federal Emergency Management Agency; 2003.
[25] Naiem F. The seismic design handbook. 2nd ed. Boston: Kluwar Academic Publishers; 2001.
[26] ASTM. Standard test methods and definitions for mechanical testing of steel products, A370-03a. ASTM International; 2003.
[27] ATC. Guidelines for seismic testing of components of steel structures report-24. Applied Technology Council; 1992.
[28] Okazaki T, Arce G, Ryu HC, Engelhardt MD. Experimental study of local buckling, overstrength, and fracture of links in eccentrically braced frames. Journal of Structural Engineering-ASCE 2005;131(10):1526–35.
[29] AISC. Seismic provisions for structural steel buildings. American Institute of Steel Construction; 2002.
[30] Richards P, Uang CM. Testing protocol for short links in eccentrically braced frames. Journal of Structural Engineering-ASCE 2006;132(8): 1183–91.
[31] Richards P, Uang CM. Effect of flange width–thickness ratio on eccentrically braced frames link cyclic rotation capacity. Journal of Structural Engineering-ASCE 2005;131(10):1546–52.
[32] HKS. ABAQUS standard user's manual. Hibbitt, Karlsson, and Sorensen, Inc; 2001.